



A Tunable Perfect THz Metamaterial Absorber with Three Absorption Peaks Based on Nonstructured Graphene

Mahdi Rahmanshahi¹ · Soheil Noori Kourani¹ · Saeed Golmohammadi¹ · Hamed Baghban¹ · Hamid Vahed¹

Received: 8 July 2020 / Accepted: 15 March 2021 / Published online: 23 March 2021
© The Author(s), under exclusive licence to Springer Science+Business Media, LLC, part of Springer Nature 2021

Abstract

In this paper, a graphene-based tunable multi-band terahertz absorber is proposed and numerically investigated. The proposed absorber can achieve perfect absorption within both sharp and ultra-broadband absorption spectra. This wide range of absorption is gathered through a unique combination of periodically cross- and square-shaped dielectrics sandwiched between two graphene sheets; the latter enables it to offer more absorption in comparison with the traditional single-layer graphene structures. The aforementioned top layer is mounted on a gold plate separated by a Topas layer with zero volume loss. Furthermore, in our proposed approach, we investigated the possibility of changing the shapes and sizes of the dielectric layers instead of the geometry of the graphene layers to alleviate the edge effects and manufacturing complications. In numerical simulations, parameters, such as graphene Fermi energy and the dimensions of the proposed dielectric layout, have been optimally tuned to reach perfect absorption. We have verified that the performance of our dielectric layout called fishnet, with two widely investigated dielectric layouts in the literature (namely, cross-shaped and frame-and-square). Our results demonstrate two absorption bands with near-unity absorbance at frequencies of 1.6–2.3 and 4.2–4.9 THz, with absorption efficiency of 98% in 1.96 and 4.62 THz, respectively. Moreover, a broadband absorption in the 7.77–9.78 THz is observed with an absorption efficiency of 99.6% that was attained in 8.44–9.11 THz. Finally, the versatility provided by the tunability of three operation bands of the absorber makes it a great candidate for integration into terahertz optoelectronic devices.

Keywords Graphene · Plasmon · Absorber · Terahertz · Metamaterial

Introduction

Terahertz (THz) radiation lies in the spectral range of 0.1–10 THz ($\sim 3\text{--}30\ \mu\text{m}$) with respective photon energies ranging from 1.24 to 12.4 meV, which falls between the microwave and mid-infrared range of the electromagnetic (EM) spectrum [1]. Ever since the emergence of the first perfect absorber proposed by Landy et al. in 2008 [2], the concept of perfect absorption has been investigated for absorbing electromagnetic waves in certain regions including visible light, infrared light, THz, and GHz [3–7]. Typically, an absorber structure consists of an upper layer, a dielectric isolation layer, and a metal layer—the combination of which forms a metal subwavelength structure [8, 9]. THz absorbers are capable of absorbing EM waves, with a

variety of applications in imaging, sensors, photo-detectors, and modulators [10–12]. Consequently, the design of such structures is of great interest. In recent years, traditional absorbers, engineered with using of natural materials, have been widely investigated [12]. The diffraction-related limitations require that the size of the device be proportional to the THz wavelength to achieve the moderate confinement of THz waves [13]; however, observing this limitation would result in undesirably large device dimensions ($\sim 0.3\ \text{mm}$ for 1 THz) and cause difficulties in device integration. At optical wavelengths, this problem is tackled with the aid of the strong coupling between EM waves and plasma oscillations at the metal surface—surface plasmon polaritons (SPPs)—to confine light in a subwavelength scale [14]. However, in the THz regime, metal behaves as a perfect electric conductor in which only a small portion of the EM energy can reside, leading to a very loosely confined surface waves [15].

As an alternative for metals, graphene has been in the center of attention during recent years to realize THz SPPs. There are three reasons to justify this: (i) graphene SPPs are

✉ Mahdi Rahmanshahi
m-rahmanshahi93@ms.tabrizu.ac.ir

¹ Faculty of Electrical and Computer Engineering, University of Tabriz, Tabriz, Iran

stimulated at THz frequencies and give improved absorption due to their resonance intensity; (ii) the graphene layers can be biased using the external gate voltage to tune the resonance frequency; and (iii) it has been already established that the absorption of a single graphene sheet is already very high (2.3% per layer) [16]. Furthermore, to enable the graphene absorbers to operate over a wide range of frequencies, the surface conductivity of graphene needs to be modified varying of its Fermi energy (E_F) using procedures such as electrostatic doping, exposure to a magnetic field, optical excitation, and controlling the gate voltage [17].

Based on these superb properties of graphene plasma, these absorbers have been studied through numerous structures of absorbers, such as the graphene nano-slits [18], the graphene micro-ribbons [19, 20], the cross-shaped graphene array [21–23], graphene metamaterial [24, 25], and graphene metasurface [26]. In practice, truncation edges created in graphene manufacturing introduce phenomena that have not been modeled in theory, collectively known as edge effects—e.g., unordered diffuse scattering losses which prevent the absorber from achieving unity absorption in practical scenarios [27]. To overcome these problems, several methods including multilayer graphene with uneven dielectric slab structure [28], graphene loaded with periodical arrays of dielectric bricks [27], and metal-dielectric-graphene sandwiched structures [29] which focus on the design of the dielectric have been proposed in the literature. Furthermore, in [30–33], the authors suggested changing the shape of the dielectric layer, which has much easier manufacturing process than structures with patterned graphene layer shape.

However, the aforementioned studies only focused on single- or dual-band absorbers. The downside of using such absorbers in THz applications is that, by structure, they can only support a limited range of the THz spectra and are not able to absorb wavelengths in the short and long THz frequency regions. However, in modern applications, the implementation of multi-band absorbers is more desired. In the literature, to realize broadband or multi-band perfect graphene-based absorbers, two design methods for their top layers are widely investigated: the first method relies on patterning composite graphene layers and metallic resonators with different shapes and sizes [34–37]; the second method dismisses the implementation of metallic resonators and instead focuses on the size and the shape of graphene layers [38–45] or dielectric layers [27, 30–32].

Ye et al. demonstrated a tunable multi-band absorber with six near-unity absorption bands from 0.1 to 10 THz using a spiral metal microstructure on a graphene sheet [34]. However, the absorbance in each band is not broad, and the absorption peak decreases as the frequency band increases. Another study in [37] proposed a hybrid absorber in which a gold disk array was placed on top of a single graphene layer with the absorption peak in 9 THz. However,

the major drawbacks of the absorbers based on the metallic structures are their fixed narrow bandwidths (BW) and post-fabrication difficulties, which render these absorbers unfavorable in practical broadband applications. T. Wang et al. [38] designed and investigated a concentric double square-ring array graphene layer and a VO_2 film layer separated by a SiO_2 layer. Their simulation results revealed that the designed absorber could provide a tunable broad absorption band from 26 to 99.2% by changing the graphene Fermi energy from 0.1 to 0.5 eV, respectively. Double-layer graphene ring arrays separated by a dielectric spacer (silica) have been shaped to achieve a dual-band absorber [39]. In [43], the authors designed a triple-band absorber with arrays of the periodically arranged graphene split ring resonators, which patterned on the dielectric layer. The absorption efficiency of this absorber is 99.57%, 99.96%, and 99.76% for resonance peaks located at 3.56 THz, 10.38 THz, and 12.96 THz, respectively. Despite the overall complicated structure, only one absorption band occurs in the main area (< 10 THz), in which none of them is wide. However, in their model, the two sharp absorption peaks only occur at a short and limited THz region (2.03 and 2.39 THz). On the other hand, L. Qi et al. [31] investigated an absorber structure consisting of uniformly spaced dielectric (SiO_2) cubes forming cross-shaped grooves on top of the graphene layer, placed on a SiO_2 layer. Their proposed absorber is able to achieve absorption with 97.8% and 31% in the range of 0.473–1.407 THz and 2.273–3.112 THz, respectively. Evidently, this structure cannot support absorption in all THz areas and only covers short frequency ranges. In [31, 38, 39, 43], SiO_2 is applied as the dielectric spacer material; however, it has been demonstrated that in THz region, Topas results in zero volume loss and constitutes a better dielectric [34].

In this paper, we propose a tunable graphene-based multi-band perfect metamaterial THz absorber with three absorption peaks of over 98% at 1.92, 4.62, and 8.81 THz with the following properties:

- We focus on varying the shape of the dielectric layer to achieve dielectric shapes with optimal refractive index ($n=2.5$) to hedge against the edge effects of the patterned graphene structures and the manufacturing problems in manipulating the graphene layers.
- We implement a two-layer graphene sandwich structure to ensure an absorption up to 90% in each band.
- We apply the Topas in the absorber structure, to minimize the volume loss.

This paper is organized as follows. In “Materials and Methods”, we present the graphene metamaterial absorber structure and express the theory behind the structure. In “Results and Discussions”, the numerical results have been

demonstrated for the proposed absorber. In “Conclusion”, the paper ends with a conclusion.

Materials and Methods

Our designed metamaterial structure consists of a patterned dielectric layer in which sandwiched between two graphene layers. In the range of THz frequencies, most natural materials cannot provide effective responses; hence, the concept of metamaterial absorbers (MAs) has been proposed as a solution; such absorbers can facilitate high absorption efficiency through the resonance in the periodical structures [17]. Metamaterials, which give us the benefit of compactness and low cost, are formed by assembling subwavelength electrically/magnetically resonant elements, which are usually arranged periodically, making it possible to modify their permittivity and permeability [46]. The aforementioned reasons have made MAs very attractive in the THz range, mostly because of their capability to achieve perfect absorption [12, 47, 48].

To achieve tunable absorption peaks in the THz region, we design a structure with three distinct layers. A 2-μm-thick gold plate was used as the bottom layer with the conductivity of $\sigma_{\text{gold}} = 4.5 \times 10^7 \text{ S/m}$, which acts as a perfect reflector in the frequency domain of interest and so, results in zero transmission coefficient [17]. The gold layer thickness is characterized regarding the corresponding skin depth value to avoid the surface current. The bottom layer is separated from the top layer by a 18-μm-thick polyethylene cyclic olefin copolymer (COC), known as Topas, which has very low losses and dispersion in the THz region [34, 49, 50]. The top layer consists of a patterned dielectric located between two graphene sheets in a sandwich pattern to obtain a multi-band absorption through continuous excitation of the graphene surface plasmons (GSPs), with corresponding geometrical parameters listed in Table 1. To minimize the reflection coefficient of the structure, the thicknesses of the separating and the upper dielectric layers are optimized to acquire impedance matching. The patterned dielectric can be realized in two different shapes: it can be patterned to include a 2-μm-thick frame-and-square dielectric, hereafter called FSD, (Fig. 1a) with refractive index of 2.5 [51, 52], or a cross-shaped dielectric, hereafter called CSD, in another (Fig. 1b).

Ultimately, two single-graphene layers are employed to construct the top layer of our MA, in which the gate electrode is connected to the upper graphene layer for DC bias connection. To realize this structure, different fabrication methods, such as photolithography on graphene and oxygen-plasma technology etching [38], growing graphene film by plasma-enhanced chemical vapor deposition (PECVD) system and employing electron beam lithography (EBL) [39],

Table 1 Geometrical sizes and descriptions of all symmetric structures: frame and square shape (FSD), cross shape (CSD), and fishnet dielectric (FND) material illustrated in Figs. 1 and 3

Geometrical parameter	Values
Length of square	$a = 8 \text{ } \mu\text{m}$
Length of the unit cell of all structures	$b = 15 \text{ } \mu\text{m}$
Width of frame and fishnet	$c = 1.5 \text{ } \mu\text{m}$
Width of cross shape	$d = 3 \text{ } \mu\text{m}$
Length of each leg of cross shape	$e = 5 \text{ } \mu\text{m}$
Gap distance	$g = 2 \text{ } \mu\text{m}$
Dielectric thickness	$td = 2 \text{ } \mu\text{m}$
Topas thickness	$ts = 18 \text{ } \mu\text{m}$
Gold thickness	$tg = 2 \text{ } \mu\text{m}$
Dielectric refractive index	$n = 2.5$ [51, 52]
Fermi energy of graphene	$E_F = 0.7 \text{ eV}$
Topas permittivity index	$\epsilon_d = 2.35$ [33, 34, 50, 59]
Gold conductivity index	$\sigma = 4.5 \times 10^7 \text{ S/m}$ [17]

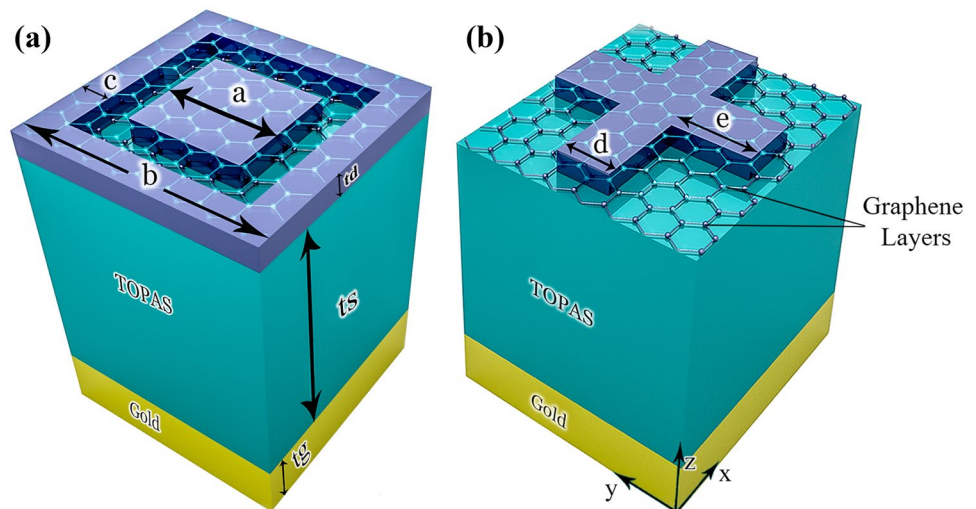
can be employed. The optical conductivity of graphene layers is expressed with the random-phase approximation (RPA) and determined by the superposition of two different optical absorption mechanisms, named intraband and interband transitions. The optical conductivity can be derived according to the Kubo formula [44] given with Eq. (1):

$$\sigma_\omega = \frac{2e^2 K_B T}{\pi \hbar^2} \frac{i}{\omega + i\tau^{-1}} \ln \left[2 \cosh \left(\frac{E_F}{2K_B T} \right) \right] + \frac{e^2}{4\hbar} \left[\frac{1}{2} + \frac{1}{\pi} \arctan \left(\frac{\hbar\omega - 2E_F}{2K_B T} \right) - \frac{i}{2\pi} \ln \frac{(\hbar\omega + 2E_F)^2}{(\hbar\omega - 2E_F)^2 + 4(K_B T)^2} \right] \tag{1}$$

where e is the electron charge, $\hbar = h/2\pi$ is the reduced Planck’s constant, K_B is the Boltzmann constant, T is the temperature, E_F is the Fermi energy of graphene, ω is the photon frequency in vacuum, and τ is the electron momentum relaxation time defined by $\tau = \mu E_F / e v_f$, in which μ is the electron mobility ($\approx 10^4 \text{ cm}^2 \text{ V}^{-1} \text{ s}^{-1}$), and v_f is the Fermi velocity (10^6 ms^{-1}). Based on the Pauli exclusion principle, the contribution of the interband between the bands can be ignored, due to low photon energy in the THz frequencies. As a result, intraband transitions are the dominant absorption phenomenon [53]. In this paper, we only consider highly doped graphene so it is assumed that $E_F \gg k_B T$ and $E_F \gg \hbar\omega$. The Kubo formula finally can be expressed as Eq. (2):

$$\sigma(\omega) = \frac{e^2 E_F}{\pi \mu^2} \frac{i}{\omega + i/\pi} \tag{2}$$

Fig. 1 Schematic illustration of a unit cell of the THz graphene-based absorber, designed on a gold substrate and Topas polymer, and composed of **a** a frame-and-square dielectric (FSD) and **b** cross-shape dielectric (CSD) material, sandwiched between two graphene layers with the geometrical parameters given in Table 1



There are two approaches to control the Fermi level: the first approach is to utilize a semiconductor substrate, e.g., silicon, to gate graphene [54], and the second method is to self-gate graphene [55]. In the latter, a patterned dielectric layer separates two single graphene layers, and, by applying a voltage between these layers, the accumulation of different types of charge carriers arises in the opposite layers. Following the injecting and depleting carriers in these layers, we can easily alter the Fermi levels. Several other methods are also discussed in the literature, such as gating graphene using ion gels [56] and doping graphene chemically [57]. Because graphene can support highly confined THz waves and its behavior in the THz region and can be actively tuned through variation of its Fermi energy, it has become one of the most popular active materials in the ultra-compact THz devices. However, in THz devices with larger sizes, where the large area graphene layers are needed, practical tunability of graphene conductivity becomes limited due to fabrication complications, which can be resolved by patterning the graphene layer or its integration with metamaterial [58].

The gold bottom layer which reflects waves and the non-structured graphene sheets loaded with periodic arrays of the patterned dielectric form the two mirrors of an asymmetric Fabry-Perot cavity, which confine EM waves and result in GSP excitation in the structure [30]. Moreover, continuous plasmon resonances provided by the patterned dielectric and graphene layers will improve the total absorption bandwidth. Hence, to obtain broad multi-band absorption, the main challenge is to find a method to broaden the GSPs. The GSP modes are excited through the structure when the wave vector of free space is equal to the wave vector of GSP expressed as follows:

$$k_{\text{GSP}}(\omega) = \frac{\pi \hbar^2}{e^2 E_f} \epsilon_0 (\epsilon_s + \epsilon_d) \omega (\omega + j\tau^{-1}) \quad (3)$$

where ϵ_0 is the permittivity of vacuum, ϵ_s is the relative permittivity of separating dielectric (Topas), and ϵ_d is the relative permittivity of periodic patterned dielectric. The wave vector in the free space is much smaller than that in graphene (k_{GSP}). Therefore, it is necessary to resolve this large difference between the two wave vectors, to facilitate GSPs excitation using incident waves from the free-space. In our approach, one of the main functions of the periodical patterned dielectric arrays is minimizing the wave vector mismatches [27]. When an x-polarized electric field (E-field) is illuminated on the absorber, its excited GSPs propagate along the same direction [30]. However, a proportion of the excited GSP modes are reflected in the interface between the top layer and the air gap, some of them are transmitted into the air and re-stimulate the GSPs in the next unit cell-since the wavelength of the illuminated E-field is much larger than the distance between the adjacent patterned dielectrics, more intense far-field interactions can be achieved [32].

In this paper, the finite-difference time-domain (FDTD) method is applied to analyze and extract the plasmonic responses of the structure. We have defined graphene as the surface current boundary condition. To save the computational time, periodic boundary conditions were set in the x- and y-directions, while perfectly matched layer (PML) boundary conditions are applied in the z-direction; therefore, several scatterings have been eliminated. The length of the selected simulation region has to be larger than half of the maximum incident wavelength to obtain convergent results using the FDTD. The incident light source in this simulation is a plane wave placed at a distance of 25 μm from the surface of the upper graphene layer and propagates in the z-direction. The proposed absorber has periodic structures, so, only one-unit cell is considered in all our simulations.

The absorption efficiency can be expressed as $A(\omega) = 1 - R(\omega) - T(\omega)$ (where $A(\omega)$, $R(\omega)$, and $T(\omega)$ represent the absorption, reflection, and transmission efficiency, respectively). The absorber will display a high absorption efficiency when $R(\omega)$ and $T(\omega)$ are both at their minimum values. The minimum value of transmission efficiency is realized when the bottom gold mirror is thick enough to inhibit all wave transmission ($T(\omega) = 0$). On the other hand, the reflection can be eliminated under certain conditions such as impedance matching of the absorber to that of the free space or satisfying the critical coupling condition. As a result, the absorption $A(\omega) = 1 - R(\omega)$ can be simply calculated from the reflection of the absorber [30].

Results and Discussions

Figure 2 shows the calculated absorption spectra of the graphene-based absorber under transverse electric (TE) polarization at normal incidence along the x -direction, with $E_F = 0.7$ eV and $\tau = 0.5$ ps. To evaluate the absorption performance of the proposed graphene-based THz absorber, we altered the geometrical parameters of the structure, separately. At first, we analyze the absorption performance of the FSD structure with only the square-like dielectric in the middle without the frame. The results (red-dashed curve) reveal that the absorber can reach nearly perfect absorption of over 95% in two regions. The first absorption band from 5.02 to 5.27 THz with maximum absorption of 96% in 5.16 THz, and the second band from 10.02 to 10.62 THz with maximum absorption of 96% in 10.34 THz. Then, the

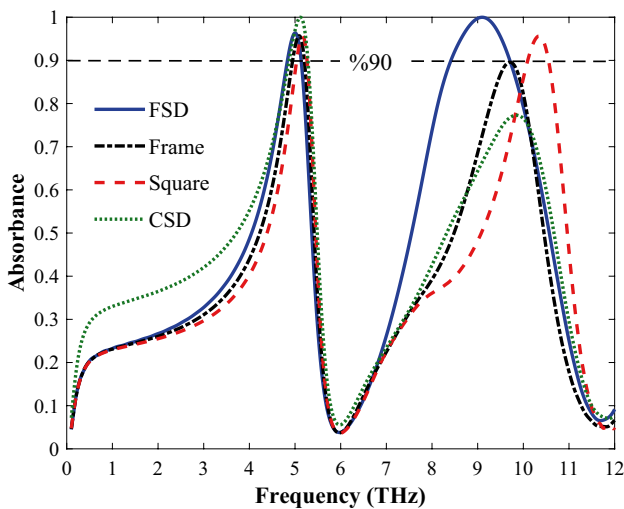


Fig. 2 The absorption spectra of the proposed structure (Fig. 1) for four different designs; frame with square known as FSD (the blue solid curve), frame with no square (the black-dashed curve), square with no frame (the red-dashed curve), and cross-shape known as CSD (the green-dashed curve)

absorption spectrum of the structure with only a frame-like dielectric (black dot and dashed curve) without squares in the middle was inspected. A shift from long frequencies to short frequencies (redshift) with the absorption of over 90% only from 9.6 to 9.8 THz in the second peak was obtained.

By combining the frame and a square in the middle of it (FSD case), a better result is obtained. In this case (blue solid curve), the first peak (with absorption above 90%) is located from 4.8 to 5.15 THz with an absorption efficiency of 97% in the center frequency (f_c) of 5.01 THz. Interestingly, the second peak faces a shift in the THz region, and the absorption efficiency of 99.9% in 9.09 THz is observed. The fractional BW and the full widths at half maximum (FWHM) are 5.8% and 1.31 THz for the first peak and 14.31% and 3.01 THz for the second peak, respectively. Finally, we consider the CSD (Fig. 1b), which, similar to the FSD, has two absorption peaks (green-dotted curve) due to the existence of GSPs at different positions. The first peak, which is larger than that of FSDs (with broad bandwidth above 90% in 4.84–5.31 THz), reaches the absorption efficiency of 99.9% at $f_c = 5.11$ THz. The fractional BW and FWHM for CSD type are 8.02% and 1.76 THz, respectively, but the second absorption peak is smaller than it is in the FSD’s counterpart, and eventually reaches a maximum of 78% at $f_c = 9.84$ THz which is not suitable for a perfect absorber.

From the results of Fig. 2, we can conclude that these simple structures can only generate two absorption peaks in the THz region. Therefore, to achieve multi-band absorption peaks, more sophisticated structures must be designed. Therefore, by combining the two previous structures, we came up with a third structure in which the cross-shaped dielectrics (CSD) were periodically aligned at equal distances. We placed a square-like dielectric in the center of

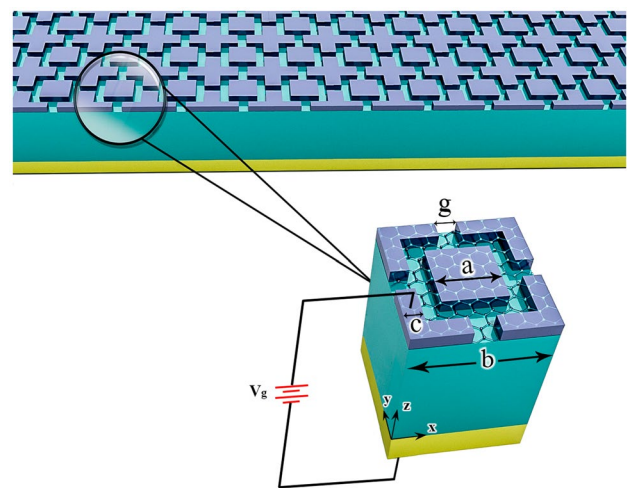


Fig. 3 Fishnet dielectric (FND) structure with a square in the middle of a fractured frame along with the geometrical parameter specifications based on Table 1

the empty spaces between the crosses (Fig. 3). Each unit cell consists of a fishnet (fractured frame) dielectric, hereafter called FND, which surrounds a square with equal spacing in its center, which causes wide variations in the absorption spectrum compared with two previous cases (Fig. 4).

In order to further performance analysis of the FND case, we separately examine the parameters' influence on our absorption spectrum for the TE polarization under normal incidence. We first investigate the absorption performance of the fractured frame structure without square in the middle. According to Fig. 4, a multi-band graphene-based absorber with three absorption peaks is constructed (the red-dashed curves), which, in the same order, correspond to the first-, second-, and third-order graphene plasmon resonances (GPRs). First absorption peak emerges in the 1.62–2.30 THz frequency region, with maximum absorption of 98.4% in 1.92 THz. Regarding the absorption spectrum, one can see that there is a cutback in absorption after 2.3 THz, and in 3.3 THz, absorption reaches a minimum of 66%. Second absorption peak appears in the 4.47 to 5.05 THz frequency region, with maximum absorption of 96% in 4.8 THz. A sharp slope is observed after 5.05 THz, reaching a minimum absorption of 7.5% in 5.95 THz. There is a third absorption peak which is broader (8.38–9.88 THz) compared with the first and the second peaks and has a maximum absorption of 92% in 9.44 THz. These absorption bands with high absorbance are achieved due to the generation of the discrete GSPs by the nonstructured graphene layers and producing a set of continuous plasmon resonances in the FND structure, along

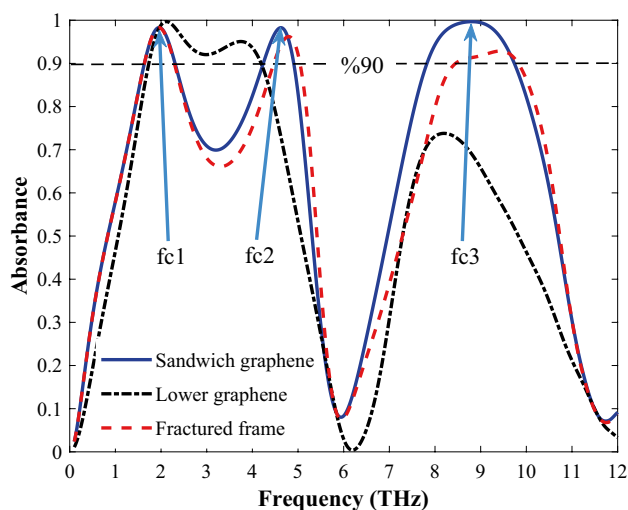


Fig. 4 The absorption spectra for the proposed structure (FND type) with three different designs. The red dashed, the black dotted and dashed, and the blue solid curves represent the fractured frame without square, the FND with only a graphene sheet under the structure (no top graphene layer), and the FND with 2 graphene layers, respectively. Here, the geometry parameters are the same as those in Table 1. Three central absorption peaks have been achieved at $fc_1=1.92$ THz, $fc_2=4.62$ THz, and $fc_3=8.81$ THz, respectively

with the complete lack of transmission and the small reflectance of the absorber in that frequency range. To enhance the absorption peaks, a square-like dielectric with dimensions of $a=8\ \mu\text{m}\times 8\ \mu\text{m}$ is placed in the middle as demonstrated in Fig. 3 (FND case). For the FND structure, first, we consider only a graphene single layer which is located under the structure. Based on the results, not only the two narrow bands are combined to form a new broad absorption band, but also the third broad absorption peak drops strongly which is not suitable for our design (black dot and dashed curve). Then, we design the optimal absorber by locating another graphene sheet at the top of the structure like a sandwich. It can be found that the 90% terahertz absorbance absolute (fractional) bandwidths of the FND graphene sandwiched structure (blue solid) are 0.68 THz (35.41%), from 1.62 to 2.30 THz, 0.66 THz (14.31%), from 4.24 to 4.9 THz, and 2.01 THz (22.81%), from 7.77 to 9.78 THz, respectively, which means the absorber is in the “ON” state. Three central absorption peaks were achieved at $fc_1=1.92$ THz, $fc_2=4.62$ THz, and $fc_3=8.81$ THz, respectively. It should also be noted that the largest reflection is 91.9% corresponding to the smallest absorptions 8.1% at 5.94 THz, which means the absorber is in the “OFF” state.

In the absorber, the graphene absorbs one part of the incident wave, which excites the propagating SPPs in the form of an evanescent wave. It is clear that the SPP's field intensity at the surface of the upper graphene layer is very strong and reveals a great absorption. Our simulation results reveal that the third absorption band broadens at longer wavelengths. Also, from another aspect, increment of the number of carriers at high Fermi energy levels ($E_F=0.7$ eV) leads to an increase in the plasma oscillation amplitude, and ultimately improves the absorption peak. In addition, there is an intense coupling between the excited SPPs on the upper and the lower graphene sheets. Moreover, the combination of the upper and the lower SPPs forms a resonator which leads to more SPP's excitation on both graphene sheets and results in enhanced field confinement and enhanced absorption. FWHM for two narrow peaks in total is 4.47 THz and for the third broader band, is 3.73 THz, which are better than the CSD and FSD structures (a detailed comparison of the performance of our proposed absorber to a number of other researches is given in Table 2).

Figure 5 demonstrates the electric field distribution on the top surface of the proposed FND at three absorption peaks in TE polarization. According to Fig. 5, the E-field distribution is mostly confined at the edges of the dielectric fractured frame layer due to the excitation of the GSPs (the red-dashed curve in Fig. 4). It should be noted that with intense confinement of the E-fields, the absorption will increase. Since the dielectric with a square shape does not have an absorption peak in 1.92 THz (the red-dashed curve in Fig. 2), therefore, the electric field is not confined around it as seen in Fig. 5a.

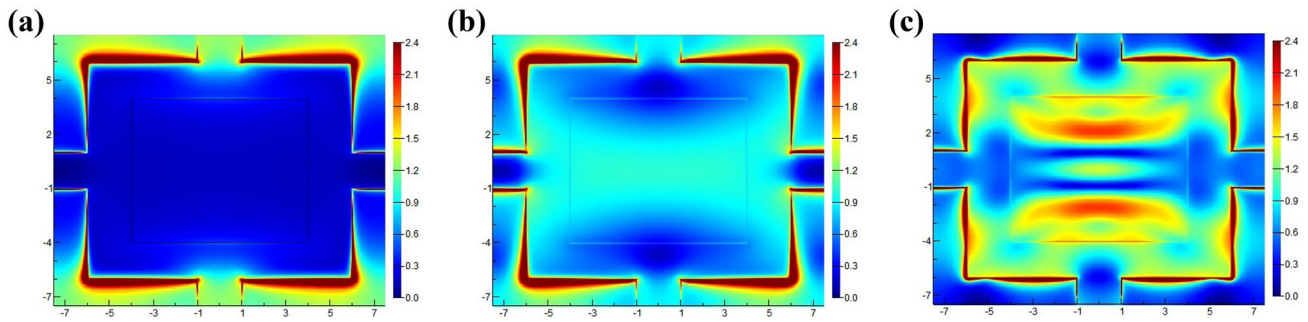


Fig. 5 Distributions of the electric field $|E|$ along the graphene surface. $|E|$ at **a** $f=1.92$ THz, **b** $f=4.62$ THz, and **c** $f=8.81$ THz for FND structure. Here, the other parameters are the same as those in Table 1

A weak E-field confinement, relative to the edges of the fractured frame, is observed around the square at 4.62 THz (Fig. 5b), which can be assigned to the first absorption peak of the absorber with only the square-shaped dielectric (Fig. 2). The E-field distribution at 8.81 THz shows a strong coupling between the fractured frame and the square edges (Fig. 5c). This is due to the strong field intensity of the excited SPPs at the edge of the graphene sheet and the coupling of them between the upper and the lower graphene sheets. Figure 5 demonstrates that only a small fraction of the incident E-field drops on the patterned dielectric layer, while the majority of the loss occurs on graphene surfaces, which implies that the GSPs in the two graphene layers play the main role in the absorption magnitude.

To investigate the effects of the geometrical parameters on the absorption of the proposed graphene-based THz absorber, we examine the absorption sensitivity to structural parameters, including Fermi level (E_F), the fishnet width (c), the fractured frame gap distance (g), the FND thickness (t_d), and the square length (a). It should be emphasized that when we change one parameter, the other geometrical dimensions are kept fixed as the initial values given in Table 1.

Tunability is one of the most important characteristics of a graphene-based absorber, where the absorption magnitude and peak frequency are tuned by manipulating the relative dielectric constant and the electric conductivity of the graphene through changing its external bias voltage. It can be inferred from Eq. (1) that the conductivity of graphene is tunable. Tuning the absorption of the proposed broadband MA is done by adjusting the Fermi energy via applying bias voltage or changing the chemical doping without altering the physical dimensions. To change the Fermi level, E_F , of the graphene, a gate voltage V_g is applied between the graphene sheet and the back gold layer. Increasing E_F causes an increase in the carrier concentration which increases the equivalent mass of the carrier collective oscillation and leads to a decrease in the damping coefficient. Therefore, for a higher chemical potential [40], the plasma oscillations will increase so that the absorption peak is considerably enhanced. A stronger local field leads to higher absorption.

The simulation results in Fig. 6 reveal that by varying the applied voltage in the graphene-dielectric-graphene structure, and variation of the Fermi energies from 0 to 0.7 eV, the absorption spectrum of the proposed absorber is tunable. It is observed that the absorption spectra decrease rapidly when E_F varies from 0.2 eV to 0 since the metallicity of graphene decreases when E_F is relatively small. Based on Fig. 6, for Fermi energies of $E_F=0$ and 0.1 eV, where there is no intensive GSPs are made, there seems to be no absorption above 90% for any frequencies, which means that the absorber is not in “ON” state. Two absorption peaks of over 90% in the frequency region of 1.4–4.9 THz are generated by increasing the Fermi energy to $E_F=0.3$ eV. With further increase in the Fermi energy, there seem to be slight changes in the broadness and the magnitude of the first absorption band (1.4–2.4 THz region), but these changes in the second peak are more noticeable, where second peaks get narrower and are blueshifted. When $E_F=0.3$ eV, we have an absorption region of 2.6 to 4.1 THz for the second peak, where an increase in the Fermi energy to 0.7 eV, shifts this absorption

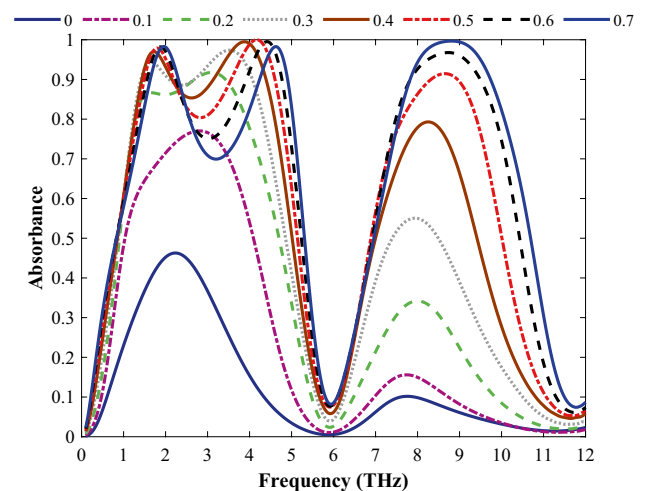


Fig. 6 The absorption spectra for FND structure (Fig. 3) with different Fermi energies (0 to 0.7 eV)

region to 4.2–4.9 THz. Since the Fermi energy increases gradually, the absorption gets intensified because of the variance of the conductivity of the graphene sheets. Figure 6 also shows that with increasing the E_F , the absorption peak magnitude of the third band also increases with a blueshift of peak frequency point. By adjusting E_F from 0 to 0.7 eV, the peak of the third absorption band raises from 10.2 to 99.6% for TE polarization. Therefore, the third broad absorption band has a switching performance in the THz region. The reason behind the increment of the absorption magnitude, with a blueshift of the peak frequency point, is: an increase in the graphene Fermi energy leads to a decrease in the real part of the relative dielectric constant of the graphene, which ultimately renders the properties of the graphene to get closer to that of a metal. Moreover, in this configuration, there is a greater chance for the incident THz wave to excite the stronger GSPs and causes a blueshift in the resonant frequency of the graphene-based absorber.

The relationship between the absorption performance of the absorber and the FND width (c) is depicted in Fig. 7. Simulation results confirm that the amplitude of the three modes gradually increases with increasing c since the distance between the adjacent unit cells becomes smaller. This notion also forms the foundation for the implementation of the FND structure of different sizes to construct a multi-band graphene-based absorber. According to Fig. 7, as the width increases, the amplitude of the first peak increases with a blueshift, while the second peak only redshifts with minor changes in its amplitude. This trend continues to the point that at $c = 2.5 \mu\text{m}$, the two absorption bands morph into one broad absorption band as the depth of the valley between them decreases. This is in agreement with the fact that increasing the fishnet width reduces the angle between two mirrors of the Fabry-Perot cavity at certain positions in the

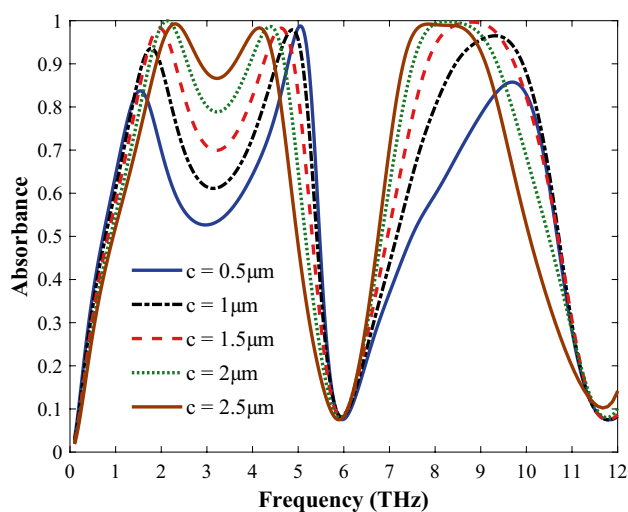


Fig. 7 The absorption spectra for FND structure with different widths of the fishnet (0.5 μm to 2.5 μm)

patterned dielectric, and eventually strengthens the corresponding resonance intensity. Ultimately, the corresponding absorption band becomes larger and narrower. The results show that with $c = 0.5 \mu\text{m}$, maximum absorption is 83% in the first peak, and for $c = 1 \mu\text{m}$, absorption changes to 93.5%, while for $c > 1 \mu\text{m}$, absorption changes to over 98%. Changing c from 0.5 to 1.5 μm causes an increase in the third absorption amplitude with a redshift, while for $c > 1.5 \mu\text{m}$, the amplitude is almost invariable. The frequency region for $c = 2.5 \mu\text{m}$ is 7.3–9.11 THz. As observed in Fig. 7, the minimum absorption of 87% in the first valley occurs around 3.2 THz. On the contrary, there are no changes in the second valley and we have absorption of 8% in 5.9 THz. This is because the surface plasmon resonance coupling between the adjacent unit cells is enhanced. Also, as the number of free electrons varies with changing c , the magnitude of the induced surface current and the full charge time of the edge region will be changed [43].

The gap distance between the different parts of the top layer is one of the key geometries that affect the absorption spectrum of the absorber. According to Fig. 8, it is worth noting that the fractured frame gap distance (g) has a great influence on the shape of the spectra and the absorption intensity. It can be found that for $g = 1 \mu\text{m}$ (blue solid), the absorbance (fractional) bandwidths of over 90% in the proposed absorber are 0.66 THz (40.7%), from 1.3 to 1.96 THz, 0.6 THz (12.76%), from 4.32 to 4.92 THz, and 1.05 THz (12.16%), from 8.13 to 9.18 THz, respectively. It is indisputable that increasing g results in two changes: firstly, the depth of the first valley and the first absorption peak amplitude in the spectrum are continually decreasing with a blueshift of the first peak. The valley between the first and the second peaks would disappear for long gap distances and cause the two absorption peaks to morph into a broader

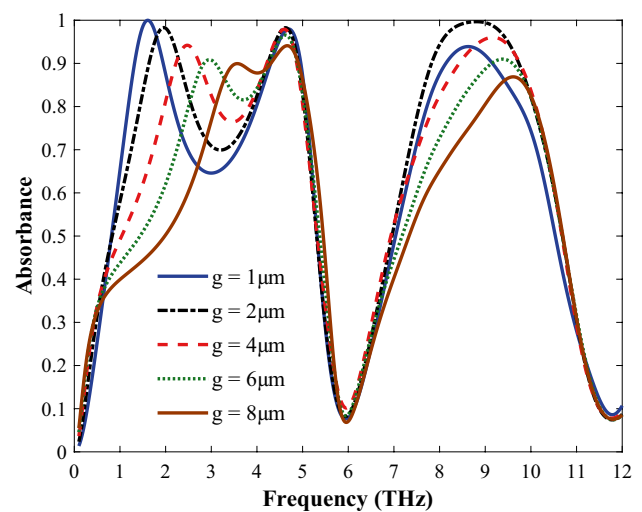


Fig. 8 The relationship between the absorption performance and the fractured frame gap distance (g) with values from 1 to 8 μm

peak. Secondly, the amplitude and absorption width of the third band experience an increase at $g = 2 \mu\text{m}$ but decrease after $2 \mu\text{m}$. Since the capacitance effect of the edge regions of the fractured frame becomes weaker, the resonance frequency shifts toward higher frequencies, and as g increases, the induced magnetic field between the two capacitors of the FND sections becomes larger. Therefore, the resonance frequency is higher for mode fc_1 and fc_2 . For mode fc_3 , the induced current on the internal component is larger than that on the external component due to the difference in the free electron population [43]. For $g = 2 \mu\text{m}$, the absorption amplitude of the three modes reaches the maximum at the same time. Therefore, the absorption of the structure will be enhanced by geometry optimization.

Another important parameter affecting the absorption curve is the dielectric thickness. As seen in Fig. 9, all three absorption peaks will experience an increase with a redshift as the thickness of FND (td) varies from 0.5 to $2 \mu\text{m}$. However, the first absorption peak drops slightly as td increases in the 2–3 μm range. Changing td alters the distance between the two graphene sheets and consequently, alters their coupling intensity and plasmon resonances which cause a shift in the absorber’s resonance frequency. With the increasing of td , the resonance frequency experiences a redshift due to the destructive surface interferences. As td increases, the impedance matching between absorber structure and free space is destroyed. Furthermore, the absorption of the absorber slightly rises with increasing coupling strength, and in our proposed absorber, when the thickness is $td = 2 \mu\text{m}$, optimum absorption is obtained where the coupling is the maximum.

Then, we investigate the effect of the square side (a) size on the absorption spectrum. Based on Fig. 10, the

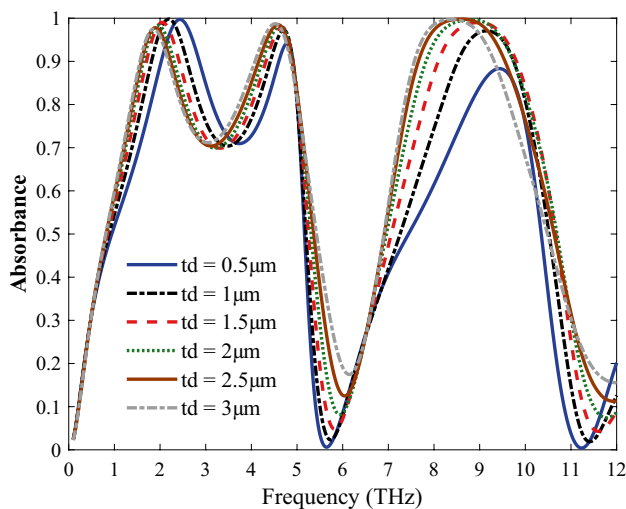


Fig. 9 The absorption spectra for FND structure with different values of the parameter td (0.5–3 μm)

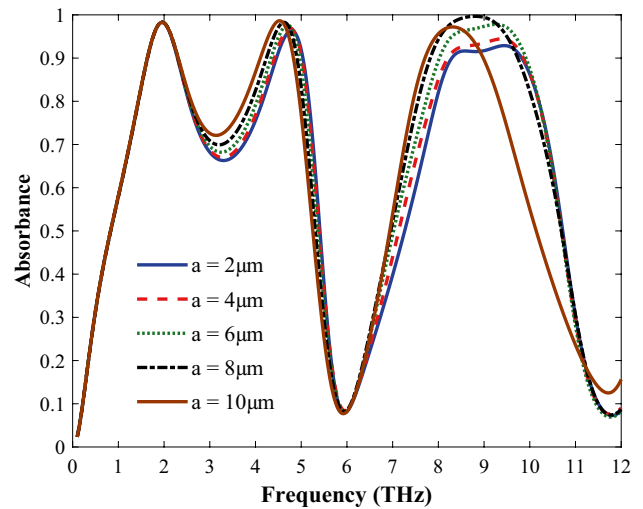


Fig. 10 The absorption spectra for FND structure with different values of the square length (a)

absorbance performance of the absorber is less sensitive to the length of the square but more sensitive to the fractured frame geometry. As the length increases, although there is no change in the first peak, the amplitude of the second and third modes gradually increases, since the distance between the fractured frame and the square becomes smaller. The most significant changes are observed in the third peak, which underlines the importance of using square dielectric. As shown in Fig. 10, for dimensions $a < 4 \mu\text{m}$, no absorption above 90% is achieved, which precludes this broad absorption band (8.2–9.87 THz range) to be regarded as an optimal absorption band. With further increase in the square side ($a > 6 \mu\text{m}$), the amplitude of the third peak increases and we

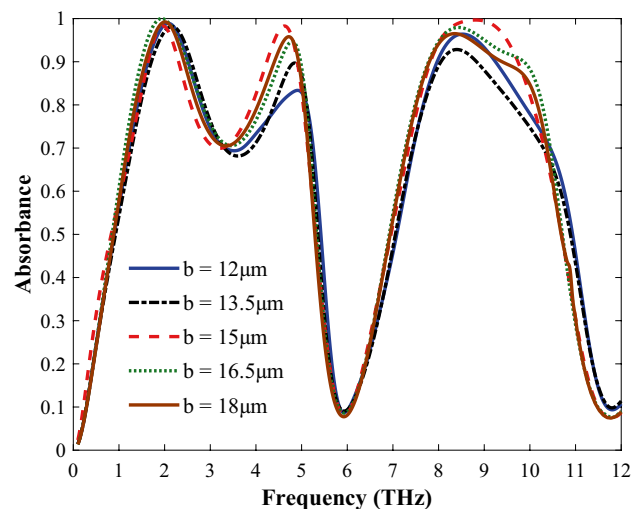


Fig. 11 Simulation results on the influence of the periodic unit size (b) of the dielectric on the absorption spectrum of the absorber for $\pm 10\%$ and $\pm 20\%$ change in the dimension

Table 2 Comparison of the present absorber with others

Ref	Type	Central frequency (THz)	Absorption	Fractional BW (%)	Structure
[37]	Single	9.15	96.9%	< 20	Periodic gold disks/graphene sheet/Au
[38]	Single	1.47	99.2%	37.41	Double graphene square rings/SiO ₂ /VO ₂
[20]	Dual	4.95, 9.2	99.8%, 99.6%	< 10	Discrete Graphene ribbon/SiO ₂ /graphene sheet/ SiO ₂ /Au
[23]	Dual	4.28, 6.85	> 99%	< 10	Cross- and disk-shaped graphene/SiO ₂ /Au/Si
[39]	Dual	2.03, 2.39	> 99%	< 10	Graphene rings/SiO ₂ /graphene rings/SiO ₂ /Au
[61]	Dual	1.6, 4.75	> 95%	31.2, 10.5	Ion-gel/discrete electrical split ring resonators (eSSR) graphene pattern/SiO ₂ /polysilicon/SiO ₂ / Au
[44]	Dual	10.02, 12.65	98.4%, 99.8%	< 10	Graphene nanoribbon-ring cross structure/SiO ₂ /Au/Si
[31]	Dual	0.92, 2.69	> 95%, > 83%	71, 29.4	Cross-shaped grooves SiO ₂ pattern/nonstructured graphene/SiO ₂ /Au
[43]	Triple	3.56, 10.38, 12.96	> 99%	< 10	Split ring resonators (SRR) graphene array/SiO ₂ /Cu
[41]	Triple	0.5, 1.64, 2.68	> 99.7%	< 10	Umbrella-shaped graphene/Si/Au
[62]	Triple	7.75, 14.85, 23.44	> 99%	< 10	Discrete graphene elliptical ring/SiO ₂ /Au
present	Triple	1.92, 4.62, 8.81	98.4%, 98.3%, 99.6%	35.41, 14.31, 22.81	Graphene sheet/square- and cross-shaped dielectric/graphene sheet/Topas/Au

get absorption of 99% for $a = 8 \mu\text{m}$. For $a = 6 \mu\text{m}$, we get a broadband frequency of 8–9.92 THz with maximum absorption of 97% in 9–9.51 THz range. In the same vein, for $a = 10 \mu\text{m}$, a broadband 7.65–9 THz with maximum absorption of 96% in the range 8–8.62 THz has been achieved. This is due to the fact that the coupling of the surface plasmon resonances between the adjacent unit cells is increased and also, as the number of free electrons changes with a , the full charge time of the edge region and the magnitude of the induced surface current is changed.

Finally, Fig. 11 presents the impact of the periodic unit (b) of the dielectric layer on the absorption performance of the proposed absorber for $\pm 10\%$ and $\pm 20\%$ change in the dimension. As it is observed from this figure, b has more influence on the peak absorption rather than the resonance frequency when the other parameters remain unchanged. In this case, the resonance conditions remain almost the same. The figure illustrates that the second mode (fc_2) redshifts slightly, and the relative absorption peak increases accordingly by increasing b from 12 to 15 μm . In addition, the third absorption peak will increase gradually but the resonance wavelength experiences blue shift, while the changes of mode fc_1 are negligible. This is because the impedance matching condition is more satisfactory and hence, the absorbance bandwidth and corresponding intensity are increased. By increasing b over than 15 μm , the maximum absorption peaks and the absorption bandwidth of the second and third modes gradually decrease. Due to the coupling between the adjacent fishnets, the resonance peak wavelength changes slightly in a small period. Also, the reduction in the absorption maximum can be attributed to a decrease in the filling ratio of graphene [60]. Results indicate that the most efficient coupling and absorption spectra are obtained for $b = 15 \mu\text{m}$.

Table 2 compares the performance of our proposed structure against conventional graphene-based THz absorbers in the literature. First and foremost, our proposed structure offers much greater absorbance bandwidth than the other works in both short and long THz frequencies. Besides, in our proposed structure, this excellent performance is achieved entailing fewer fabrication complications as the model focuses on modifying the geometry of the dielectric rather than the graphene layers.

Conclusion

In summary, we have proposed and simulated a tunable nonstructured graphene-based perfect THz metamaterial absorber with multi-band absorption. Our proposed absorber showed perfect absorption within ultra-broadband absorption spectra, which is realized through a structure whose top layer is consisted of a fishnet Topas dielectric (FND) sandwiched between two graphene sheets to obtain absorption through continuous excitation of GSPs. In our simulations, we observed the role of different geometrical and physical parameters including Fermi level, the fishnet width, the fractured frame gap distance, the FND thickness, and the square length in the characteristics of the absorbance spectra. More specifically, we focused on the resultant changes in the absorption amplitude, bandwidth, peak central frequencies, FWHM, and E-field distribution to reach the optimal absorber structure. Our proposed FND structure can realize multi-band absorption with over 90% absorbance at three frequency regions (central frequencies): 1.62–2.30 THz ($fc_1 = 1.92 \text{ THz}$), 4.24–4.90 THz ($fc_2 = 4.62 \text{ THz}$), and 7.77–9.78 THz ($fc_3 = 8.81 \text{ THz}$), with the absorption efficiencies of 98.4%, 98.3%, and

99.6%, respectively. In this structure, the multi-band absorption can be attributed to the Fabry-Perot cavity between the top layer and the underneath metal reflector as well as the far-field interactions between the adjacent unit cells. In the same vein, the broad bandwidth and the high amplitude peak of the realized absorption spectrum can also be attributed to the impedance matching between the free space and the absorber. The current work can be further improved by exploring the possibility of the implementation of an unstructured dielectric plate sandwiched between two graphene layers underneath the current proposed FND to increase the absorption regions.

Authors Contribution All of the authors have the same contribution percentages in this manuscript. M. Rahmanshahi and S. Noori Kourani have performed the simulations, S. Golmohammadi, H. Baghban, and H. Vahed have contributed in discussions and writing the materials. All co-authors have seen and agree with the contents of the manuscript and they certify that the submission is original work and is not under review at any other publication.

Funding This article has no funding. The authors received no financial support for the research, authorship, and/or publication of this article.

Data Availability The data and materials of this manuscript are available after publishing.

Code availability The simulation files are available for reviewers upon request.

Declarations

Conflict of Interests The authors declare no competing interests.

References

- Arezoomandan S et al (2017) Graphene-based reconfigurable terahertz plasmonics and metamaterials. *Carbon* 112:177–184
- Landy NI et al (2008) Perfect metamaterial absorber. *Phys Rev Lett* 100(20):207402
- Wang X et al (2019) A theoretical study of a plasmonic sensor comprising a gold nano-disk array on gold film with a SiO₂ spacer. *Chin Phys B* 28(4):044201
- Chen X et al (2019) Magnetic properties and reverse magnetization process of anisotropic nanocomposite permanent magnet. *J Magn Magn Mater* 483:152–157
- Liu Z et al (2019) Truncated titanium/semiconductor cones for wide-band solar absorbers. *Nano technology* 30(30):305203
- Van Huynh T et al (2019) Controlling the absorption strength in bidirectional terahertz metamaterial absorbers with patterned graphene. *Comput Mater Sci* 166:276–281
- Tang J et al (2018) Calculation extinction cross sections and molar attenuation coefficient of small gold nanoparticles and experimental observation of their UV–vis spectral properties. *Spectrochim Acta Part A Mol Biomol Spectrosc* 191:513–520
- Wang X et al (2019) Surface-enhanced Raman scattering by composite structure of gold nanocube-PMMA-gold film. *Opt Mater Express* 9(4):1872–1881
- Zhang Q et al (2019) One-dimensional Fe₇S₈@ C nanorods as anode materials for high-rate and long-life lithium-ion batteries. *Appl Surf Sci* 473:799–806
- Dorodnyy A et al (2018) Plasmonic photodetectors. *IEEE J Sel Top Quantum Electron* 24(6):1–13
- Guo Y et al (2018) Chip-integrated geometric metasurface as a novel platform for directional coupling and polarization sorting by spin-orbit interaction. *IEEE J Sel Top Quantum Electron* 24(6):1–7
- Peng L et al Metal and graphene hybrid metasurface designed ultra-wideband terahertz absorbers with polarization and incident angle insensitivity. *Nanoscale Advances*, 2019.
- Andryieuski A, Lavrinenko AV, Chigrin DN (2012) Graphene hyperlens for terahertz radiation. *Phys Rev B* 86(12):121108
- Ding W, Andrews S, Maier S (2007) Internal excitation and superfocusing of surface plasmon polaritons on a silver-coated optical fiber tip. *Phys Rev A* 75(6):063822
- Maier, S.A., *Plasmonics: fundamentals and applications*. 2007: Springer Science & Business Media.
- Amin M, Farhat M, Bağcı H (2013) An ultra-broadband multi-layered graphene absorber. *Opt Express* 21(24):29938–29948
- Zhou Q et al (2018) Controlling enhanced absorption in graphene metamaterial. *Opt Commun* 413:310–316
- Cai Y et al (2015) Enhanced spatial near-infrared modulation of graphene-loaded perfect absorbers using plasmonic nanoslits. *Opt Express* 23(25):32318–32328
- Khavasi A (2015) Design of ultra-broadband graphene absorber using circuit theory. *JOSA B* 32(9):1941–1946
- Xing R, Jian S (2018) A dual-band THz absorber based on graphene sheet and ribbons. *Opt Laser Technol* 100:129–132
- Ke S et al (2015) Plasmonic absorption enhancement in periodic cross-shaped graphene arrays. *Opt Express* 23(7):8888–8900
- Xiao B, Gu M, Xiao S (2017) Broadband, wide-angle and tunable terahertz absorber based on cross-shaped graphene arrays. *Appl Opt* 56(19):5458–5462
- Zhang J, Tian J, Li L (2018) A dual-band tunable metamaterial near-unity absorber composed of periodic cross and disk graphene arrays. *IEEE Photonics J* 10(2):1–12
- Wang F et al (2018) Dual-band tunable perfect metamaterial absorber based on graphene. *Appl Opt* 57(24):6916–6922
- Zhou Q et al (2018) Multi-band terahertz absorber exploiting graphene metamaterial. *Opt Mater Express* 8(9):2928–2940
- Rahmanzadeh M, Rajabalipannah H, Abdolali A (2018) Multi-layer graphene-based metasurfaces: robust design method for extremely broadband, wide-angle, and polarization-insensitive terahertz absorbers. *Appl Opt* 57(4):959–968
- Gao F et al (2017) Broadband wave absorption in single-layered and nonstructured graphene based on far-field interaction effect. *Opt Express* 25(9):9579–9586
- Xu B-Z et al (2013) A novel structure for tunable terahertz absorber based on graphene. *Opt Express* 21(20):23803–23811
- Wang Z, Hou Y (2017) Ultra-multiband absorption enhancement of graphene in a metal-dielectric-graphene sandwich structure covering terahertz to mid-infrared regime. *Opt Express* 25(16):19185–19194
- Yang J et al (2018) Broadband terahertz absorber based on multi-band continuous plasmon resonances in geometrically gradient dielectric-loaded graphene plasmon structure. *Sci Rep* 8(1):1–8
- Qi L, Liu C, Shah SMA (2019) A broad dual-band switchable graphene-based terahertz metamaterial absorber. *Carbon* 153:179–188
- Nourbakhsh M, Zareian-Jahromi E, Basiri R (2019) Ultra-wideband terahertz metamaterial absorber based on Snowflake Koch Fractal dielectric loaded graphene. *Opt Express* 27(23):32958–32969
- Nourbakhsh M et al An Ultra-Wideband Terahertz Metamaterial Absorber Utilizing Sinusoidal-Patterned Dielectric Loaded Graphene.

34. Ye L et al (2019) Composite graphene-metal microstructures for enhanced multiband absorption covering the entire terahertz range. *Carbon* 148:317–325
35. Meng K et al (2019) Tunable broadband terahertz polarizer using graphene-metal hybrid metasurface. *Opt Express* 27(23):33768–33778
36. Guo T, Jin B, Argyropoulos C (2019) Hybrid graphene-plasmonic gratings to achieve enhanced nonlinear effects at terahertz frequencies. *Phys Rev Appl* 11(2):024050
37. Cheng R et al (2020) Tunable graphene-based terahertz absorber via an external magnetic field. *Opt Mater Express* 10(2):501–512
38. Wang T et al (2020) Dual-controlled switchable broadband terahertz absorber based on a graphene-vanadium dioxide metamaterial. *Opt Mater Express* 10(2):369–386
39. Su W, Chen X, Geng Z (2019) Dynamically tunable dual-frequency terahertz absorber based on graphene rings. *IEEE Photonics J* 11(6):1–8
40. Qi Y et al (2019) Tunable plasmonic absorber in THz-band range based on graphene “arrow” shaped metamaterial. *Results Phys* 15:102777
41. Li J-S, Sun J-Z (2019) Umbrella-shaped graphene/Si for multi-band tunable terahertz absorber. *Appl Phys B* 125(9):183
42. Liu Z, Guo L, Zhang Q (2019) A simple and efficient method for designing broadband terahertz absorber based on singular graphene metasurface. *Nanomaterials* 9(10):1351
43. Cen C et al (2019) Theoretical design of a triple-band perfect metamaterial absorber in the THz frequency range. *Results in Physics* 14:102463
44. Yi Z et al (2019) Nanoribbon-ring cross perfect metamaterial graphene multi-band absorber in THz range and the sensing application. *Results in Physics* 14:102367
45. Jin X et al (2019) Coherent perfect absorber with independently tunable frequency based on multilayer graphene. *Opt Commun* 446:44–50
46. He J, Zhang Y (2017) Metasurfaces in terahertz waveband. *J Phys D Appl Phys* 50(46):464004
47. Cui Y et al (2014) Plasmonic and metamaterial structures as electromagnetic absorbers. *Laser Photonics Rev* 8(4):495–520
48. Zhao X et al (2016) Nonlinear terahertz metamaterial perfect absorbers using GaAs. *Photonics Res* 4(3):A16–A21
49. Jena R et al (2010) Viscosity of COC polymer (TOPAS) near the glass transition temperature: experimental and modeling. *Polym Testing* 29(8):933–938
50. Ye L et al (2018) Electrically tunable broadband terahertz absorption with hybrid-patterned graphene metasurfaces. *Nanomaterials* 8(8):562
51. Zalkovskij M et al (2012) Ultrabroadband terahertz spectroscopy of chalcogenide glasses. *Appl Phys Lett* 100(3):031901
52. Ramachari D et al (2019) High-refractive index, low-loss oxyfluorosilicate glasses for sub-THz and millimeter wave applications. *J Appl Phys* 125(15):151609
53. Rahmanshahi M et al Infrared photodetectors based on graphene metal nano clusters. *Photonics and Nanostruct-Fund and App*, 2018. 31: p. 173–179.
54. Sensale-Rodriguez B et al (2012) Broadband graphene terahertz modulators enabled by intraband transitions. *Nat Commun* 3:780
55. Sensale-Rodriguez B et al (2011) Unique prospects for graphene-based terahertz modulators. *Appl Phys Lett* 99(11):113104
56. Ju L et al (2011) Graphene plasmonics for tunable terahertz metamaterials. *Nat Nanotechnol* 6(10):630
57. Bae S et al (2010) Roll-to-roll production of 30-inch graphene films for transparent electrodes. *Nat Nanotechnol* 5(8):574
58. Grigorenko A, Polini M, Novoselov K (2012) Graphene plasmonics *Nat photonics* 6(11):749
59. Huang X et al (2019) Metamaterial absorber with independently tunable amplitude and frequency in the terahertz regime. *Opt Express* 27(18):25902–25911
60. Cen C et al (2020) A dual-band metamaterial absorber for graphene surface plasmon resonance at terahertz frequency. *Phys E* 117:113840
61. Hu N et al (2018) Dual broadband absorber based on graphene metamaterial in the terahertz range. *Opt Mater Express* 8(12):3899–3909
62. Yi Z et al (2019) Graphene-based tunable triple-band plasmonic perfect metamaterial absorber with good angle-polarization-tolerance. *Res Phys* 13:102149

Publisher's Note Springer Nature remains neutral with regard to jurisdictional claims in published maps and institutional affiliations.